Spatially weighted mutual information image registration for image guided radiation therapy

Samuel B. Park
Department of Radiation Oncology, Case Western Reserve University School of Medicine, 10900 Euclid Avenue, Cleveland, Ohio 44106

Frank C. Rhee
School of Electrical Engineering and Computer Science, Hanyang University, 1271 Sangrok-gu Sa-3-dong, Ansan, Gyeonggi 426-791, Republic of Korea

James I. Monroe
Medical Physics Services Ltd., 430 Saddlespur Road, Webster Groves, Missouri 63119

Jason W. Sohn[a]
Department of Radiation Oncology, Case Western Reserve University School of Medicine, 10900 Euclid Avenue, Cleveland, Ohio 44106

Purpose: To develop a new metric for image registration that incorporates the (sub)pixelwise differential importance along spatial location and to demonstrate its application for image guided radiation therapy (IGRT).

Methods: It is well known that rigid-body image registration with mutual information is dependent on the size and location of the image subset on which the alignment analysis is based [the designated region of interest (ROI)]. Therefore, careful review and manual adjustments of the resulting registration are frequently necessary. Although there were some investigations of weighted mutual information (WMI), these efforts could not apply the differential importance to a particular spatial location since WMI only applies the weight to the joint histogram space. The authors developed the spatially weighted mutual information (SWMI) metric by incorporating an adaptable weight function with spatial localization into mutual information. SWMI enables the user to apply the selected transform to medically "important" areas such as tumors and critical structures, so SWMI is neither dominated by, nor neglects the neighboring structures. Since SWMI can be utilized with any weight function form, the authors presented two examples of weight functions for IGRT application: A Gaussian-shaped weight function (GW) applied to a user-defined location and a structures-of-interest (SOI) based weight function. An image registration example using a synthesized 2D image is presented to illustrate the efficacy of SWMI. The convergence and feasibility of the registration method as applied to clinical imaging is illustrated by fusing a prostate treatment planning CT with a clinical cone beam CT (CBCT) image set acquired for patient alignment. Forty-one trials are run to test the speed of convergence. The authors also applied SWMI registration using two types of weight functions to two head and neck cases and a prostate case with clinically acquired CBCT/MVCT image sets. The SWMI registration with a Gaussian weight function (SWMI-GW) was tested between two different imaging modalities: CT and MRI image sets.

Results: SWMI-GW converges 10% faster than registration using mutual information with an ROI. SWMI-GW as well as SWMI with SOI-based weight function (SWMI-SOI) shows better compensation of the target organ's deformation and neighboring critical organs' deformation. SWMI-GW was also used to successfully fuse MRI and CT images.

Conclusions: Rigid-body image registration using our SWMI-GW and SWMI-SOI as cost functions can achieve better registration results in (a) designated image region(s) as well as faster convergence. With the theoretical foundation established, we believe SWMI could be extended to larger clinical testing. © *2010 American Association of Physicists in Medicine.*
[DOI: 10.1118/1.3463609]

Key words: spatially weighted mutual information, image registration, image guided radiation therapy, and mutual information

I. INTRODUCTION

Multiple imaging procedures for patient treatment planning are increasing and image guided radiation therapy (IGRT) has become the *de facto* standard for radiotherapy.[1] The typical IGRT procedure requires the registration (also commonly referred to as "alignment") of a point-of-delivery image with a previously generated target image. These registrations usu-

ally occur between different imaging modalities, for example, registering a conventional CT used for planning the patient's treatment with a cone beam CT (CBCT) used for patient positioning prior to treatment. Since multimodal image registration used in IGRT is by far the dominant application, we concentrate our efforts here. By comparing the images captured prior to a daily radiation treatment to the images used for the radiation therapy plan, a transformation is generated by which the patient can be correctly positioned (usually in the form of patient shifts and rotations). Computerized computational alignment methods have been developed to either fully or partially automate these processes, which is collectively known as image registration.[2]

Image registration is formally described as the process of aligning an image set (source/reference image) to another image set (acquired/test image), which has different spatial coordinates. Through image registration, we obtain transform parameters from one image coordinate system to a different image coordinate system. If the transform parameters are Euclidean transformations, they preserve the shape of the image. Such a transformation is called a "rigid-body transformation." For three-dimensional images, rigid-body image registration usually computes translations (along the x, y, and z axes) and rotations (around the x, y, and z axes), yielding six possible parameters which act on the entire data set. However, deformable image registrations employ multiple voxel-dependent distortions in addition to the translation and rotation.[3–5] Typical IGRT systems use various implementations of rigid-body image registration.[6,7]

I.A. Mutual information

A general explanation for all readers of the basic concepts relevant to this paper follows, while technical discussions are presented in Sec. II.

To find out the optimal transformation parameters using an automated process, image registration utilizes similarity measures to determine when two images have achieved the optimal outcome (best alignment). Mutual information (MI) is one such similarity measure and can be simply described in the following example. When presented with two supposedly orthogonal images, say an anterior-posterior (AP) image and a lateral image of a patient, the information provided by the pair of images can be used to align the patient to a position in space. But after examining and aligning the images, it is determined that a mistake has been made and the images are actually two AP images. Information needed to position the patient has been lost. By aligning the images, you reduced the amount of information they represented. The images did not contain different information, they contained the same, or "mutual," information. Extending this reasoning solely to the task of aligning images, it is apparent that the amount of mutual information shared between two images is maximized to achieve the best registration between the images.

The concept of mutual information was introduced to medical image registration by Collignon and colleagues and Viola and Wells in approximately 1994.[8,9] Since that time,

mutual information has become the most important measure in the vast application of registration in medical imaging. Pluim *et al.*[10] published a 2003 review of mutual information as applied to medical image registration and cited over 160 references. Since two image sets can be acquired from different modalities (MRI, CT, PET, etc.), pixel values representing the same tissue can differ from image to image set. Mutual information is useful as it works with image sets acquired from different modalities.

A central concept in relating differing images is based on the "entropy" of image, which can be addressed without explicitly dealing with positional information. Entropy is calculated in histogram space by first binning the pixels by their values (say 256 bins for a gray scale image). Divide each bin by the total number of image pixels, so now you have fractions that represent the probability of each pixel value occurring in the image p_r (gray value). Multiply this probability by its log and sum the results

$$\tilde{H} = -\sum_{k=1}^{L} p_r(r_k)\log p_r(r_k). \tag{1}$$

By extending this simple idea to a pair of images (and using a joint histogram space), one can formulate the degree of alignment between two images. The image modes and absolute pixel values are not important, only their statistical relation.

I.B. Rigid-body registration with regions of interest

In normal circumstances, tissues and organs are always changing and moving. Thus, it is impossible to achieve a perfect match between two *in vivo* image sets and we cannot build a perfect *in vivo* image registration. It is often desired to have a better match in a region of interest (ROI), even if this induces a loss of similarity in less "important" image areas. Many studies have suggested the use of "a ROI" to perform rigid-body image registration using mutual information as a cost function.[6,11,12] For clarity purposes, we will refer to registrations using mutual information as a cost function as "MI registration." Since MI registration considers only the image portion within the ROI and all pixels within the ROI with equal importance, there are a few problems. First, if a ROI includes only the treatment targets, this can lead to misalignment of the neighboring critical organs falling outside the ROI. Second, some organ structures which have significant image features (uniform intensity and steep intensity gradient), such as bone and skin, which overly influence the registration result. That is, an image registration result characterized by MI is much dependent on the location and size of the ROI.

I.C. Weighted mutual information and mutual information with spatial information

Some investigators have proposed a form of weighted mutual information (WMI) image registration.[13,14] The WMI approach corrects the effect of overly dominant image features described above by applying smaller weights to the

extreme pixel values. However, this method does not completely resolve the first problem because the weights are applied in the joint histogram space instead of geometrical image space; the differential weight values are globally applied to all of the ROI area. Therefore, it is impossible to assign the spatial distribution of the weights relative to specific pixel location.

Some have investigated the use of additional spatial information (i.e., gradient information) with MI or entropy.[15–18] These approaches can achieve better registration results than MI when either image set is blurred or for a biased MRI.[19] However, since they are utilizing gradient information, the higher gradient surfaces such as bone and skin surfaces will dominate the registration result. These approaches also require extra computation time to calculate the gradient similarity or image segmentation.

In radiation therapy, it is preferential to align two images in the region where the treatment target and neighboring critical organs are located. Recently, Wilkie *et al.*[20] utilized the modified weighted mutual information to set the weight between MI of the whole image and MI of a ROI. This method allows the user to find a negotiated transform between the registration of whole image and the registration of a small ROI. However, the method only allows two importance weights: c for the MI of the whole image and $(1-c)$ for MI of the ROI. Moreover, this method requires two calculations of MI.

I.D. Spatially weighted mutual information

We will derive a new metric for image registration that incorporates the (sub)pixelwise differential importance along spatial location without increasing computational complexity. We are modifying the mutual information measure and proposing spatially weighted mutual information (SWMI), where various weight values can be applied in the geometrical image space, not in joint histogram space. Since we formulated SWMI to incorporate any kind of weight function, we will limit this investigation to a Gaussian-shaped weight function (GW) and a structures-of-interest (SOI) based weight function to demonstrate SWMI with IGRT applications.

The remainder of this paper is organized as follows. First, we describe how mutual information is applied for image registration. Second, we derive the spatially weighted mutual information measure from mutual information. In addition, we show how our spatially weighted mutual information is used for image guided radiation therapy. We introduce a Gaussian-shaped weight function and a SOI-based weight function. Finally, we present the proof-of-concept test results of our image registration method on one synthetic example and four real patients.

II. MATERIALS AND METHODS

II.A. Image representation and mutual information

Let digital image $f(\mathrm{x})$ be described by a set of discrete samples $f_i = f(\mathrm{x}_i)$, $\mathrm{x}_i \in V$, which is defined on discrete domain

V. The pixel values at points between the integer grids can be calculated by an interpolation scheme. Therefore, we can describe the image $f(\mathrm{x})$ on the continuous domain. Image registration is the process that aligns a test image $f_T(\mathrm{x})$ to a reference image $f_R(\mathrm{x})$. We assume these two images are continuous, defined on the continuous domain V_T and V_R, respectively. Let $g(\mathrm{x}|\mu)$ be the transform from the point x on domain V_T to the domain V_R, which is transformed by μ parameters. We can describe the image registration as the optimization process to align the transformed test image $f_T(g(\mathrm{x}|\mu))$ with the reference image $f_R(\mathrm{x})$. This optimization process is defined as seeking the optimum parameter μ that minimizes a similarity function S as

$$\hat{\mu} = \arg \min_{\mu} S(f_R(\mathrm{x}), f_T(g(\mathrm{x}|\mu))). \tag{2}$$

Mutual information has been recognized as a good image similarity measure due to its robustness and multimodal capability.[6,10,21–23] If we assume $p(k)$ to be the probability of k, the joint Shannon entropy of two images is defined as

$$H(f_R, f_T) = -\sum_l \sum_k p(l,k|\mu) \cdot \log_2 p(l,k|\mu), \tag{3}$$

where $p(l,k|\mu)$ is the joint probability.[23] Then, mutual information of the two images can be defined as

$$I(f_R, f_T) = H(f_R) + H(f_T) - H(f_R, f_T)$$

$$= \sum_l \sum_k p(l,k|\mu) \cdot \log \frac{p(l,k|\mu)}{p(k) \cdot p(l|\mu)}. \tag{4}$$

To apply mutual information to an optimization process, Thévenaz and Unser[22] introduced the Parzen window joint probability. They utilized B-spline kernel functions as a Parzen window. Mattes *et al.*[24] also used this method. Computing time can be reduced by grouping pixel values within a bin through utilizing the Parzen window method. This also reduces noise by smoothing the histogram. Now, let k be a histogram bin index of the reference image, not a grayscale value and let l be a histogram bin index of the test image. Let f_R^0 and f_T^0 be the minimum grayscale values of the reference image and test image, respectively. In addition, let Δb_R and Δb_T be the range of the grayscale values for each bin of the reference image and test image, respectively. Then, the Parzen window joint probability can be given as

$$p(l,k|\mu) = \alpha \sum_{\mathrm{x} \in V} \beta^{(0)} \left(k - \frac{f_R(\mathrm{x}) - f_R^0}{\Delta b_R} \right)$$

$$\cdot \beta^{(3)} \left(l - \frac{f_T(g(\mathrm{x}|\mu)) - f_T^0}{\Delta b_T} \right), \tag{5}$$

where $\beta^{(0)}$ is the zero-order spline Parzen window, $\beta^{(3)}$ is the cubic spline Parzen window, and α is a normalization factor that guarantees $\sum p(l,k) = 1.0$.[22]

II.B. Spatially weighted mutual information

Since the mutual information measure is calculated in histogram space, we modified the joint probability by adding

differential importance throughout the geometrical image space. By adding a weight term $w(\mathrm{x})$ in the joint probability, the spatially weighted joint probability can be described as

$$p_w(l,k|\mu) = \alpha_w \sum_{\mathrm{x} \in \mathbf{V}} w(\mathrm{x}) \cdot \beta^{(0)}\left(k - \frac{f_R(\mathrm{x}) - f_R^0}{\Delta b_R}\right)$$
$$\cdot \beta^{(3)}\left(l - \frac{f_T(\mathrm{g}(\mathrm{x}|\mu)) - f_T^0}{\Delta b_T}\right), \tag{6}$$

where α_w is the normalizing constant such as α in Eq. (5). We set higher weights to important image regions, so that $p_w(l,k)$ is more dependent on the particular image region. However, less important image regions do not dictate $p_w(l,k)$ since $w(\mathrm{x})$ is lower. Since mutual information is computed with the sum of $p(l,k)$ and the weighting function is defined on the domain of the reference image, we can rewrite the marginal probability of each image and mutual information as

$$p_w(l|\mu) = \sum_k p_w(l,k|\mu), \tag{7}$$

$$p_w(k) = \sum_l p_w(l,k|\mu) = \alpha_w \sum_{\mathrm{x} \in \mathbf{V}} w(\mathrm{x})\beta^{(0)}\left(k - \frac{f_R(\mathrm{x}) - f_R^0}{\Delta b_R}\right), \tag{8}$$

and

$$I_w(f_R, f_T) = \sum_l \sum_k p_w(l,k|\mu) \cdot \log_2 \frac{p_w(l,k|\mu)}{p_w(k) \cdot p_w(l|\mu)}, \tag{9}$$

respectively. Then, SWMI $I_w(f_R, f_T)$ has more dependency on higher weighted image regions. This means that the SWMI has higher values when the higher weighted image region is aligned better.

To use SWMI as a cost function for optimizing process, we need a gradient of SWMI cost function. Though we modified the joint probability equation, we can follow the similar process of MI. Let S_w be $-I_w$, then the SWMI cost function S_w can be written as a function of μ.

$$S_w(\mu) = -\sum_l \sum_k p_w(l,k|\mu) \cdot \log_2 \frac{p_w(l,k|\mu)}{p_w(k) \cdot p_w(l|\mu)}. \tag{10}$$

Since $w(\mathrm{x})$ does not alter the characteristics of B-spline Parzen window mutual information such as the partition of the unity, the gradient of the SWMI can be derived as Eq. (11) which is the same form as MI's.

$$\frac{\partial S_w}{\partial \mu} = -\sum_l \sum_k \frac{\partial p_w(l,k|\mu)}{\partial \mu} \cdot \log_2 \frac{p_w(l,k|\mu)}{p_w(l|\mu)}. \tag{11}$$

Detailed derivations of the gradients of MI were illustrated in a reference listed.[22]

Finally, we can describe the derivative of spatially weighted joint probability as

$$\frac{\partial p_w(l,k|\mu)}{\partial \mu} = \frac{\alpha_w}{\Delta b_T} \sum_{\mathrm{x} \in \mathbf{V}} w(\mathrm{x})\beta^{(0)}\left(k - \frac{f_R(\mathrm{x}) - f_R^0}{\Delta b_R}\right)$$
$$\cdot \frac{\partial \beta^3(u)}{\partial u}\bigg|_{u=l-\frac{f_T(\mathrm{g}(\mathrm{x}|\mu))-f_T^0}{\Delta b_T}}$$
$$\cdot \left(-\frac{\partial f_T(t)}{\partial t}\bigg|_{t=\mathrm{g}(\mathrm{x}|\mu)}\right)^T \cdot \frac{\partial \mathrm{g}(\mathrm{x}|\mu)}{\partial \mu}. \tag{12}$$

Detailed derivation of the spatially weighted joint probability is described in the Appendix. The gradient of the SWMI cost function and the derivative of the spatially weighted joint probability show that the important image regions with higher weights affect the gradient of the cost function more, which accelerates the optimization and reduces the oscillation caused by less important image regions.

II.C. Determination of the weight distribution function

The weight function $w(\mathrm{x})$ can be determined by the user. Since we have already derived a general form of gradients, any shape of the weight function can be utilized depending on the application. In this study, we presented two types of weight functions for IGRT applications. One is Gaussian-shaped weight function and the other is a SOI weight function.

II.C.1. Gaussian-shaped weight function

For radiation treatment images, the target tumor area is usually the most important. The central axis of the radiation beam and the gantry axis of rotation cross at isocenter. While making a radiation treatment plan, this isocenter is usually placed in the tumor volume. Radiation beams are determined relative to this isocenter. Therefore, radiation imaging devices attached to radiation treatment machines (such as a cone beam CT) are also using the same isocenter point as a default image center. As a result, image regions near isocenter coincide with the tumor volume. In addition, there is less scatter noise near the isocenter point since it is the center of image.[25,26] So we prefer to choose a Gaussian-shaped weight distribution centered at isocenter as our weight function for IGRT. This Gaussian-shaped weight distribution provides three benefits. One benefit is that the weights near isocenter are higher so the importance of that area can be taken into account. Another benefit is the ease in controlling the boundary of the weight function. Since the outer area of the boundary defined by two times the standard deviation (2σ) includes only 5% of the weight, we can intuitively and visually check the outer boundary of region to be calculated. Finally, we can compensate the deformation of the outer region with the gradual decreasing weight of the Gaussian function. Therefore, our image registration is neither dominated by, nor neglects the neighboring critical organs.

II.C.2. SOI weight function

Another possible weight distribution for IGRT is to use one or more SOI to define the weight function. Radiation
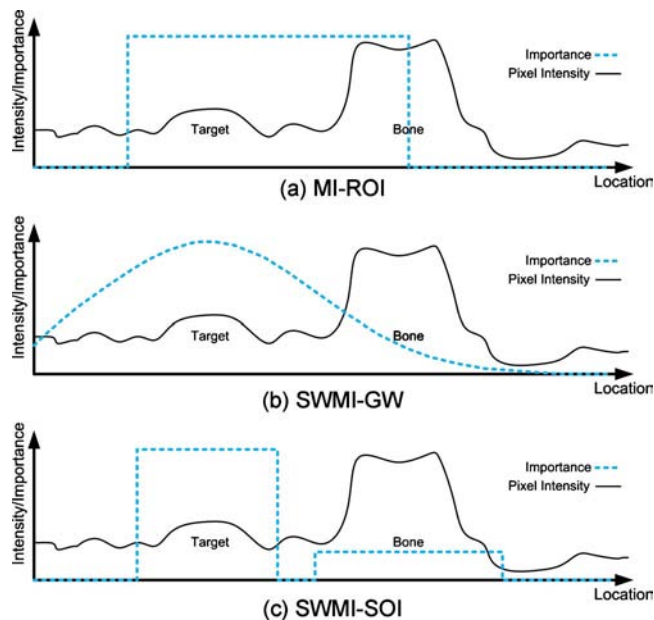
FIG. 1. Illustration shows the difference between MI registration with ROI (MI-ROI) and SWMI. Intensity is shown in one-dimensional image. (a) A specific region is selected for MI-ROI. (b) A Gaussian weight function allows us to assign different weights throughout a selected region for SWMI registration (SWMI-GW). (c) SWMI registration with ROI-based weight (SWMI-SOI) allows us to set the different weights on the different ROIs.

oncologists draw (or "contour") the organs, targets, and other relevant structures on the planning CT images used for the radiation treatment plan. To use these image structures for registration, we can select any combination of the contours and assign "importance" rankings to them for registration. If a satisfactory contour or set of contours does not exist, the SOI can simply be created by directly drawing them. SWMI allows us to set different importance rankings (or weights) to the various SOI.

Our scheme for the SOI-based weight function is to set higher weights on the important SOIs, such as CTV and critical organs at risk (OARs) and lower weights on the mobile bones. As an example, for head and neck patients, we can set the weight 1.0 for the CTV, 0.8 for the parotid glands, and 0.4 for the mandible.

When we apply the weight on the SOIs, we expand the SOI contours. Because the contour is drawn on the edge of the organ or SOI, the contour boundary does not include enough image features adversely affecting the registration. We apply a small expansion (5–10 mm) if a SOI is large enough and includes clear edges (i.e., bone structure). For soft tissue organs (i.e., rectum, bladder, parotid, and submandible glands), a 10–20 mm expansion is applied since their image features are usually not sufficient.

II.D. Term summary: MI-ROI, SWMI-GW, and SWMI-SOI

We illustrate the conceptual difference between the conventional MI and SWMI in Fig. 1. As shown in Fig. 1(a), a selected area carries the same importance weight for MI registration. However, when a Gaussian-shaped weight function

is used in SWMI, we can set a gradient importance to the image region as shown in Fig. 1(b). When we set different weights to different SOIs, SWMI can utilize a SOI-based weight function, which is shown in Fig. 1(c). We refer to image registration utilizing MI with a ROI as MI-ROI, image registration using SWMI with a Gaussian-shaped weight function as SWMI-GW, and image registration using SWMI with a SOI-based weight function as SWMI-SOI.

II.E. Experimental setup

Image registrations were performed on a Dell precison 690 workstation (Intel Xeon dual core 2.66 GHz with 6 GB RAM) running 64 bit GNU/Linux. The Insight Tool Kit is used as the optimization library.[27] The registration software was compiled with the Gnu Compiler Collection version 4 compiler. Image sets are imported as DICOM data sets (image set, isocenter, and segmented organ contours).

A gradient descent optimizer is used for image registration. Gradient descent is general and fast with first order gradients.[28] A multiresolution approach was not considered for this study. In fact, since the patient was positioned for imaging by using lasers which were installed in the treatment room, the patient was already positioned within a convergence range. Therefore, the multiresolution approach was not necessary.

Two 2D synthetic images (a reference image and a test image) were generated to provide a precision initial test of the SWMI registration method. The artificial image includes a body, a target, an OAR, two small bones, and two mobile bones. We simulated the patient displacement, organ deformation, and noise in the images. The reference image was modified by adding 2% noise and the test image was modified by adding 5% noise. The body was displaced 7.0 mm to left (a transverse shift). The target was rotated 8.0°. The OAR was shrunk by 10% and translated 2.0 and 1.0 mm to the left and in the posterior direction, respectively. Two mobile bones were translated 7.0 mm in the posterior direction. Figure 2 shows the synthesized images and the deformation map. Figures 2(a) and 2(b) show the reference image and the test image, respectively. Figure 2(c) shows the difference image between the reference image and the test image. In difference images, a gray area means no difference and the white and black areas mean a maximum difference. Figure 2(d) shows the deformation map which was applied for simulating internal organ deformation.

Four different tests were performed to compare the registration. The first test was MI-ROI registration with the ROI defined by $X: 100$ mm and $Y: 60$ mm. The second was MI-ROI registration with a ROI defined by $X: 180$ mm and $Y: 140$ mm. The third was SWMI-GW. For SWMI-GW, the Gaussian center was chosen at the center of the ROI for MI registration. And the Gaussian variances were set at $\pm 2\sigma = (X: \pm 90$ mm and $Y: \pm 70$ mm). And the last was SWMI-SOI. We set the 1.0 weight for the target, 0.8 weight for the OAR, 0.4 weight for the small bones, and 0.15 weight
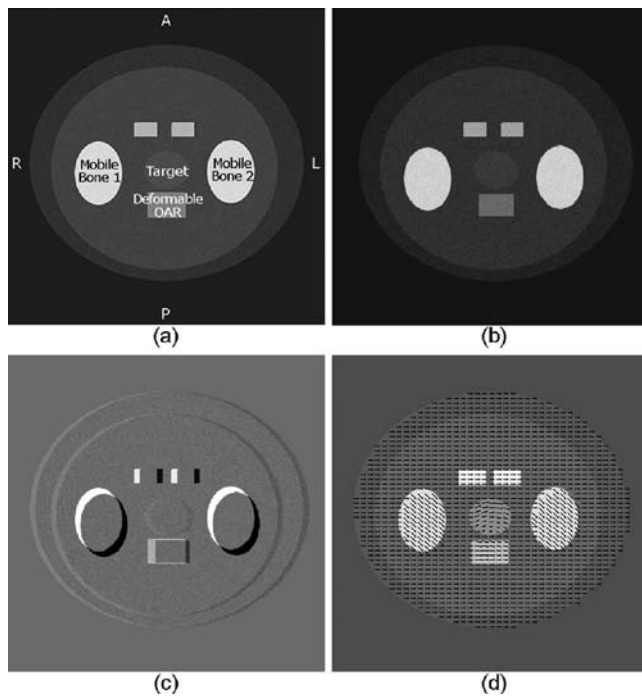
FIG. 2. Synthetic CT image sets were utilized to test image registration: (a) Reference image and (b) test image. (c) Difference image between reference and test image. (d) Deformation fields are displayed with an arrow overlaid on the reference image. Reference and test image sets were added with 2% and 5% noise, respectively. Organ deformation was simulated as follows: Total body is translated by 7.0 mm to the left direction. Target is rotated 8.0°. Deformable OAR is scaled −10% and translated by (2.0, 1.0 mm) to the left and posterior direction, respectively. Mobile bones were translated by 7.0 mm to the posterior direction.

for the mobile bones. SOI contours were expanded as much as 15 mm for the target, 10 mm for the OAR, and 5 mm for the others.

Four patient treatment data sets were also used for our studies. One set was a prostate cancer patient and the others were head and neck cancer patients. The prostate cancer patient had nine kilovoltage CBCT image sets during a 10-week treatment. We utilized one CBCT image set out of the nine sets to test the convergence and the robustness of the SWMI-GW registration. The reference image was a conventional CT data set of the prostate patient used for radiation treatment planning and the test image set was a CBCT image set. We tested 41 different initial translational offsets. The

offsets were arbitrarily selected between −15 and +15 mm on each spatial axis. The reference image was a conventional CT data set of the prostate cancer patient used for radiation treatment planning and the test image set was a CBCT image set of the same patient. The convergence and robustness was tested using two methods: MI-ROI and SWMI-GW. For the SWMI-GW registrations, the isocenter was chosen to be a Gaussian weight center. The Gaussian variances were assigned $\pm 2\sigma$ $=(X: \pm 120$ mm, $Y: \pm 90$ mm, and $Z: \pm 50$ mm). For comparison, the mutual information registration was performed using the same ROI.

We used the same patient image sets to validate SWMI-GW and SWMI-SOI registration methods. The same GW function was used as the above test for SWMI-GW. SWMI-SOI registration for the prostate case used the following SOI: Prostate, seminal vesicles, bladder, rectum, and the femoral heads. The weight and expansion for SWMI-SOI were illustrated in Table I.

One of the head and neck patients had a tumor at the right parotid and had seven CBCT image sets taken during a 7-week treatment. One of the seven CBCT sets was used to validate two image registration methods proposed in our study. The first registration test was performed using SWMI-GW with a Gaussian weight distribution centered at the radiation beam isocenter. The variances were set to $\pm 2\sigma=(X: \pm 80$ mm, $Y: \pm 80$ mm, and $Z: \pm 100$ mm). SWMI-SOI was tested with the SOI set consisting of the CTV, left parotid, submandibular glands, mandible, spinal cords, and the brain stem. The weight and expansion for SWMI-SOI were illustrated in Table I.

The third patient had three CTVs in the neck area around spine and had 35 helical megavoltage CT (MVCT) scans. SWMI-GW and SWMI-SOI registration were tested with one chosen MVCT image set which was taken on 31st day after the planning CT. Since the Tomotherapy plan has no isocenter information, we chose a point near the center of the primary CTV as a center of the Gaussian weight for SWMI-GW. The variances were set to $\pm 2\sigma$ $=(X: \pm 100$ mm, $Y: \pm 90$ mm, and $Z: \pm 60$ mm). For SWMI-SOI the SOI set of CTVs, parotids, mandible, spinal cords, and the brain stem were chosen. The weight and expansion for SWMI-SOI were summarized in Table I.

TABLE I. Summary of weight values and expansion of SOI for SWMI-SOI.

Prostate			Head and neck			Head and neck (MVCT)		
Structure	Margin (mm)	Weight	Structure	Margin (mm)	Weight	Structure	Margin (mm)	Weight
Prostate	15	1.00	CTV	15	1.00	CTV1	8	1.00
Seminal vesicles	15	1.00	Parotid glands	10	0.90	CTV2 and CTV3	6	0.90
Bladder and rectum	10	0.40	Mandible	5	0.50	Mandible	5	0.50
Femoral heads	5	0.15	Cord	10	0.60	Cord	10	0.50
			Brain stem	10	0.60	Brain stem	10	0.40
						Parotid glands	8	0.80

The last patient's image sets were employed to test our software for CT and MRI image fusion. This patient had an irregular shaped tumor in the left maxillary. Since tissue density information is necessary for radiation dose calculations, a CT image set is acquired for radiation therapy planning. However, since MRI images often provide superior resolution between tumor and normal tissue, the image fusion of CT and MRI image sets can be a key technology for precise tumor delineation. Although CT images and MRI images may be taken with the patient positioned identically, it is almost impossible to acquire the same patient internal anatomical position in both CT and MRI images. Therefore, a robust image fusion method is required to use the imaging modalities together and exploit their assets. We used the SWMI-GW registration method and set the center of the Gaussian weight to the isocenter which was located in the tumor, and the variances were set to $\pm 2\sigma = (X: \pm 80$ mm, $Y: \pm 90$ mm, and $Z: \pm 100$ mm).

III. RESULTS

III.A. Synthetic 2D image test

Figure 3 shows the comparison of four registration tests. The left column of Fig. 3 shows the reference image overlaid with different ROI setups. The right column shows the difference images between the reference image and the registered test images. In Fig. 3(a), MI registration with a small ROI on target shows that the target deformation dominated the whole registration and it compromised the other organs. A difference image shows a perfect match on the target but the mobile bones and OAR were misaligned by 20.6 and 8 mm, respectively. However, as shown in Fig. 3(b), MI registration with a larger ROI was influenced by the mobile bone although the bone occupies only 19% of the ROI region. The difference image shows the good match on the mobile bones but the target was misaligned as much as 7 mm.

Figure 3(c) shows the result of SWMI-GW. SWMI-GW with the variance $\pm 2\sigma = (X: \pm 90$ mm and $Y: \pm 70$ mm) shows a well negotiated alignment. The difference image shows the target and OAR were aligned within 3 mm and the mobile bones were aligned within 7 mm. Gaussian-shaped weight distribution is displayed on the reference image in color scale.

The result of SWMI-SOI registration is shown in Fig. 3(d). SOI-based weight distribution is shown on the reference image. SWMI-SOI registration aligned the target and OAR within 2 mm and the mobile bones with in 7 mm.

III.B. Application to a prostate patient (CBCT)

Figure 4 shows the convergence of translation and rotation parameters per iteration during optimization. Figure 4(a) is the plot of the translational convergence of 41 trials using MI-ROI registration and Fig. 4(b) is the plot of translational convergence using SWMI-GW registration. Figure 4(c) is the plot of rotational convergence using MI-ROI registration and Fig. 4(d) is the plot of rotational convergence using
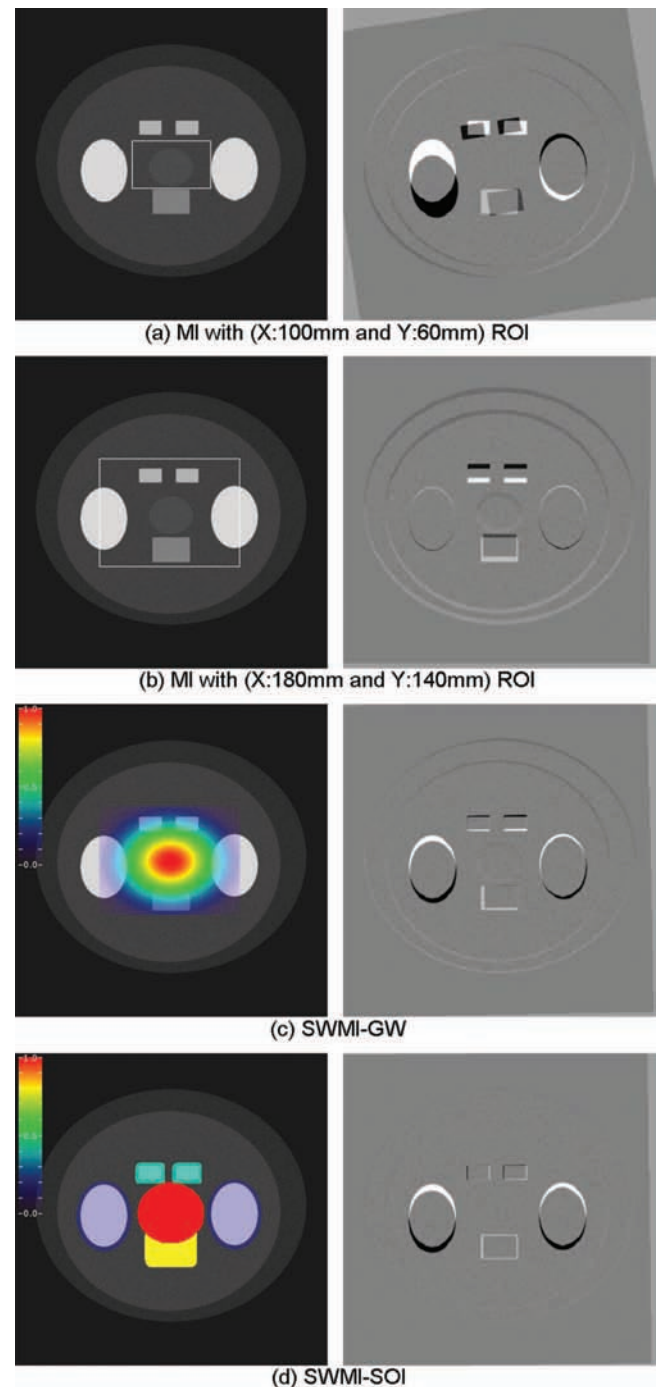

(a) MI with (X:100mm and Y:60mm) ROI

(b) MI with (X:180mm and Y:140mm) ROI

(c) SWMI-GW

(d) SWMI-SOI

FIG. 3. Registration result comparison. (a) A result of MI registration with (X:100 mm and Y:60 mm) ROI on target. (b) A result of MI registration with (X:180 mm and Y:140 mm) ROI. (c) A result of SWMI-GW registration with $\pm 2\sigma = (X: \pm 90$ and $Y: \pm 70$ mm) ROI. (d) A result of SWMI-SOI registration with the expanded contours. The left column shows the reference image overlaid with the respective ROI. The colored weight map was displayed for SWMI-GW and SWMI-SOI. The right column shows the difference images between the reference image and the registered test images.

SWMI-GW registration. Mobile femur or rectum deformation created oscillations during optimization. MI-ROI registration required an average of 40.6 iterations and SWMI-GW registration required 36.4 iterations to converge.
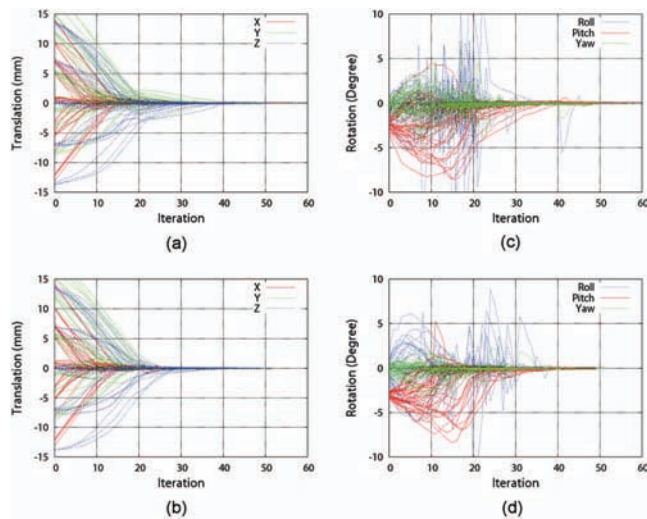
FIG. 4. Comparison of registration convergences with 41 translational offsets using a prostate treatment image set. (a) Translational convergence in x, y, and z axes as the iteration progresses with MI-ROI registration. (b) Translational convergence in x, y, and z axes with SWMI-GW registration. (c) Rotational convergence in pitch, yaw, and roll as the iteration progresses with MI-ROI registration. (d) Rotational convergence in pitch, yaw, and roll with SWMI-GW registration.

Figure 5 shows a result of the image registrations using SWMI-GW. Figure 5(a) is the planning CT image with the contour. Figure 5(b) shows the cone beam CT has the smaller field of view. Figure 5(c) shows the checkerboard image to validate the result of SWMI-GW with a

Gaussian function boundary with $\pm 2\sigma$ $=(X:\pm 120 \text{ mm}, Y:\pm 90 \text{ mm}, \text{ and } Z:\pm 50 \text{ mm})$ displayed as a red rectangle. Figure 5(d) shows the SWMI-SOI result. Both of the SWMI-GW and SWMI-SOI results shows a comparable match of the targets.

III.C. Application to a head and neck patient (CBCT)

Figures 6(a) and 6(b) are showing the reference image and the test image, respectively. A cone beam CT in Fig. 6(b) has much noise and artifacts. The Gaussian function boundary with the variances $\pm 2\sigma$ $=(X:\pm 60 \text{ mm}, Y:\pm 80 \text{ mm}, \text{ and } Z:\pm 100 \text{ mm})$ is shown as a red rectangle in Fig. 6(c). The result of the SWMI-GW registration shows that both the tumor volume and the bone are matched well. The SWMI-SOI registration result is shown in Fig. 6(d). SWMI-SOI also produces a comparable result to that of SWMI-GW.

III.D. Application to head and neck with multiple CTVs (MVCT)

Figures 7(a) and 7(b) are showing the reference image and the test image, respectively. Three CTVs are shown as contours on the images. The checkerboard image result of SWMI-GW registration is shown in Fig. 7(c). The result of SWMI-SOI registration is shown in Fig. 7(d). Both of SWMI-GW and SWMI-SOI shows that all of three tumor volumes as well as spine are matched well.
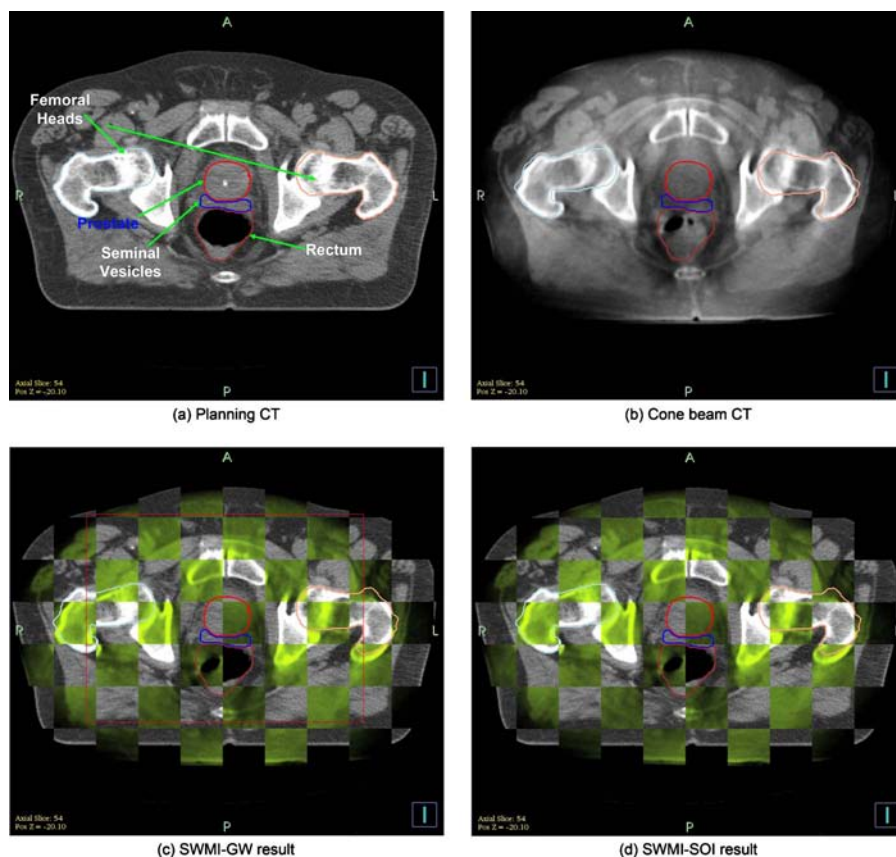

FIG. 5. Image registration result for a prostate patient. (a) Planning CT with the ROI overlaid. (b) A cone beam CT of 36th day after the planning CT is acquired. (c) The registration result of SWMI-GW with the weight centered at beam isocenter. The rectangular box shows the $\pm 2\sigma$ boundary for SWMI-GW registration. (d) The result of SWMI-SOI registration.
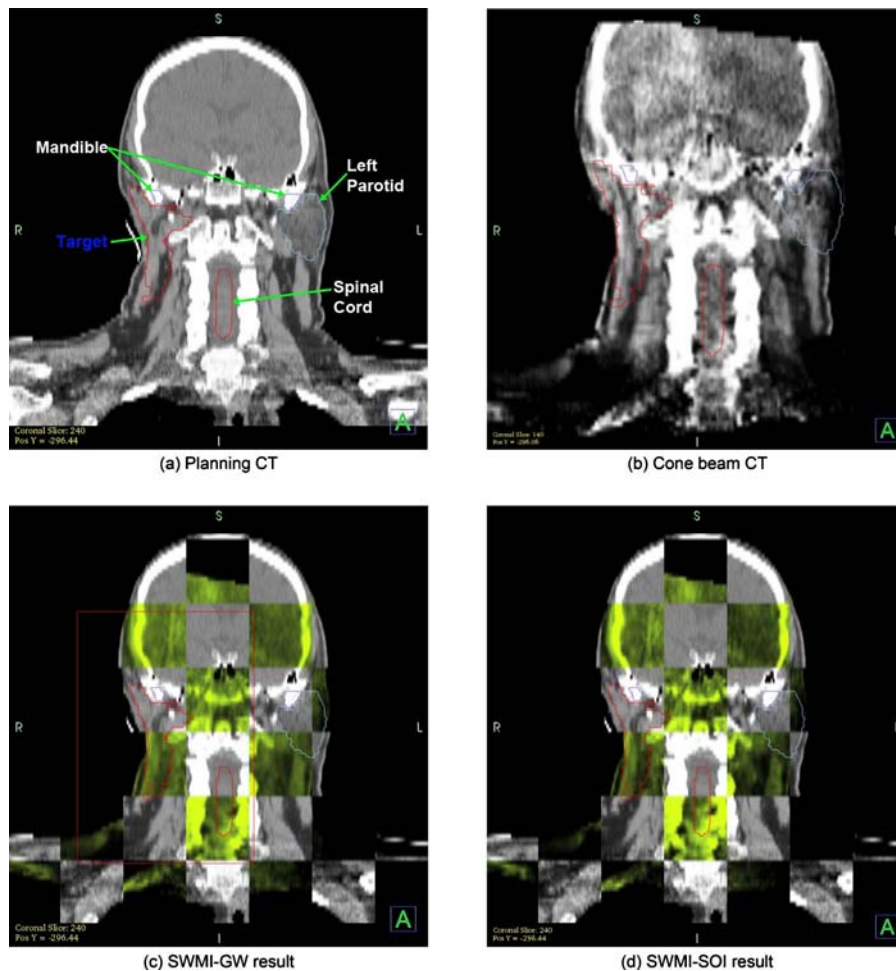
FIG. 6. Image registration result for a head and neck image set. (a) Planning CT image with the ROI overlaid. (b) A cone beam CT of 28th day after the planning CT is taken. (c) The registration result of SWMI-GW with the weight centered at beam isocenter. The rectangular box shows the $\pm 2\sigma$ boundary for SWMI-GW registration. (d) The result of SWMI-SOI registration.

III.E. Image fusion test of CT and MRI

Images of a patient with a tumor in the left maxillary are presented in Fig. 8. The red crosshair is the isocenter point picked by a physician. As shown in Fig. 8, our proposed image registration shows good alignment around the tumor area in spite of the anatomical deformations that occurred in the spine and skin surface.

IV. DISCUSSIONS AND CONCLUSION

By deriving a technique to apply a user-defined weight function in geometric image space to mutual information, we provide image registration the ability to adjust the differential importance over the image region. Many image registration trials were performed with various weight sets for SWMI-SOI and multiple boundary sizes for SWMI-GW. For SWMI-GW, we tested 3528 registrations for the nine prostate cases with a range of $\pm 2\sigma$ from $(X: \pm 80, Y: \pm 70, Z: \pm 30$ mm$)$ to $(X: \pm 160, Y: \pm 110, Z: \pm 70$ mm$)$ and 1575 registrations for the head and neck case with a range of $\pm 2\sigma$ from $(X: \pm 60, Y: \pm 50, Z: \pm 70$ mm$)$ to $(X: \pm 120, Y: \pm 110, Z: \pm 140$ mm$)$. From these trials, optimal results in the tested registrations with SWMI-GW suggest two general rules for defining the center and variance of Gaussian-shaped weight functions.

(1) Head and neck cancer case: The Gaussian center should be located near or at the tumor volumetric center and the $\pm 2\sigma$ boundary should be set on the distal edge of spine relative to the tumor.
(2) Prostate case: The Gaussian center should be located near or at the prostate volumetric center and $\pm 2\sigma$ boundary is set on the center of the femoral heads.

We also tested SWMI-SOI with various combinations of weights (0.05–1.0) and expansions (3, 5, 8, 10, 15, and 20 mm) of the SOIs. Our test results suggest that the general rules for assigning weights and expansions of the SOIs.

(1) Head and neck cancer case: A small CTV should have the highest weight (1.0) and expanded by 15–20 mm. If the CTV is large, expansion can be small as 10 mm. If the CTV is not a primary one, then the weight can be lower than the weight of the primary CTV (i.e., 0.9). Other critical soft tissue organs should have high weights (0.7–0.9) and the contours expanded by 10–15 mm. Bone SOI should have the lowest weight (≤ 0.5) and should be expanded by 5–10 mm.
(2) Prostate case: Prostate and seminal vesicles should have the highest weight (1.0) with 15–20 mm expanded contours. Bladder and rectum should have a midrange
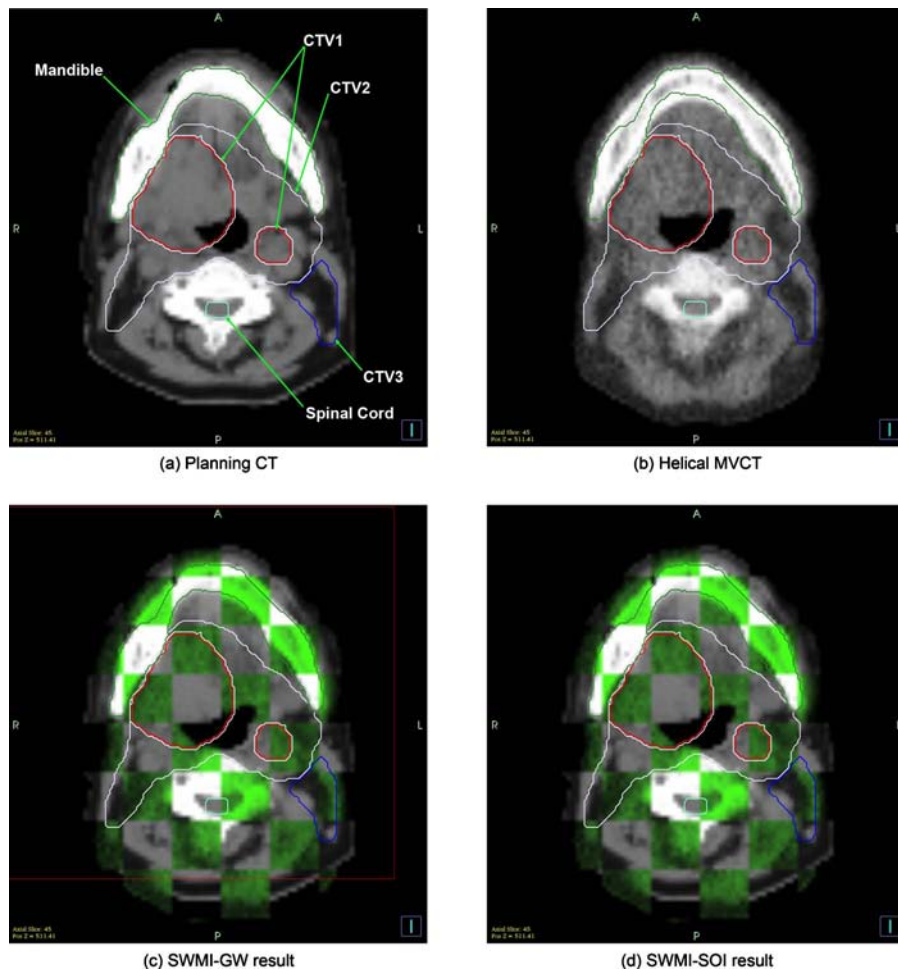
FIG. 7. Image registration result for a head and neck image set with three CTVs. (a) Planning CT image with the contours of CTVs overlaid. (b) A helical MVCT of 31st day after the planning CT is taken. (c) The registration result of SWMI-GW. The rectangular box shows the $\pm 2\sigma$ boundary for SWMI-GW. (d) The registration result of SWMI-SOI.

weight (0.6–0.8) and 10–15 mm expanded contours. Femoral heads should have a very low weight (≤ 0.2) with 5 mm or less expanded contours.

Because the test images for IGRT are acquired within a convergence range, a multiresolution method is not required. However, we believe our method should be applied with pyramid image structures for the applications that have different coordinate systems, which produce a large displacement between those image sets.[29]

Though we added a multiplication of the weight function in the joint probability equation, computational complexity did not increase. We could premultiply the weight values and the Parzen-windowed function values for the pixels in reference images. Both MI-ROI and SWMI-GW registrations took about 10 s for our tests. SWMI-SOI registrations took about 1 min. SOI expansion procedures for SWMI-SOI caused extra computation time. Though we presented two types of weight distribution for SWMI; a Gaussian-shaped weight and a SOI-based weight, we can utilize SWMI with
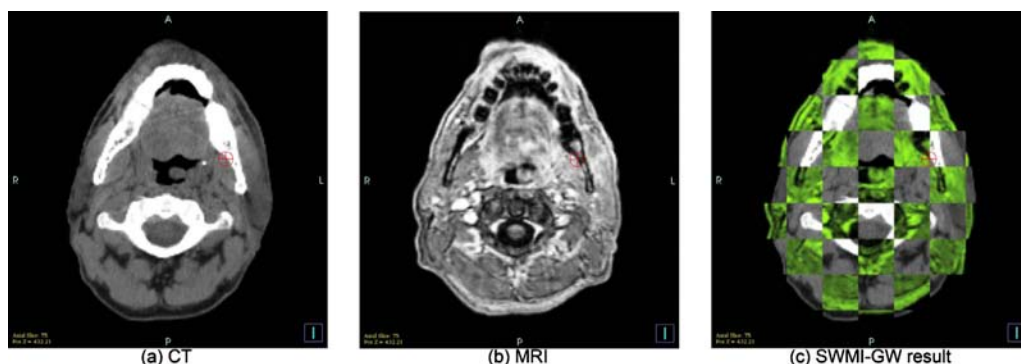

FIG. 8. Image registration result between MRI and CT using SWMI-GW. The crosshair is the tumor isocenter. (a) CT, (b) MRI, and (c) the registration result of SWMI-GW.

other image registration applications by selecting an appropriate weight distribution function. Some examples of the weight distributions are as follows:

(1) If there are several tumor volumes, we can apply the superposition of multiple Gaussian functions.
(2) If we want to trace rectal movement, we can apply a ring shaped weight function in order to avoid the interference from rectal filling.
(3) If we wish to have a specific pixel value dominate or influence at least the registration in the reference image which is similar to WMI, we can apply a weight distribution that is as a function of pixel value $w(f(\mathrm{x}))$.
(4) If we want to focus on the surface matching, we can apply a weight function that is dependent on the pixel value gradient $w(\partial f(\mathrm{x}))$.

We believe SWMI is an adaptable similarity measure for multimodality image registration.

We examined SWMI-GW and SWMI-SOI results with the gradient descent optimizer. We understand that the gradient descent optimizer may not be the best one. When SWMI-SOI suffers from a lack of image feature caused by inadequate SOI contour expansions, about one case of ten could not converge to the point of maximal metric value. Therefore, we also tested the limited memory Broyden–Fletcher–Goldfarb–Shanno (L-BFGS) optimizer.[30] The L-BFGS optimizer could be a solution for better convergence. However, both of the gradient descent and the L-BFGS optimizers proved their effectiveness with adequate contour expansions.

We have initiated small clinical retrospective studies comparing SWMI to existing registrations and reported the preliminary results.[31] Determining the variances of Gaussian weight functions and determining the weights of SOIs for clinical applications need further research. Moreover, Boswell *et al.*[7] showed that even with a phantom image, manual registration led the misalignment up to 4.2 mm and 3°. Judgment of patient registration results is much more subjective. Therefore, a broader clinical and statistical study is essential. Using our SWMI-GW and SWMI-SOI, a user can repeat the automatic registration by slightly changing the weight parameter instead of manual adjustment. On the other hand, MI-ROI registration is greatly influenced by a change

of ROI. We are pursuing more experience and testing to provide an optimized library of weight functions for specific treatment sites so that we can achieve the ultimate goal of automatic registrations without human intervention.

We have proposed an enhanced rigid-body image registration method using SWMI. We successfully derived SWMI using spatially weighted joint probability.

Since the capability of handling multimodal images is inherited from mutual information, our SWMI can be used for multimodal image registration.

In the presence of tissue deformation, rigid-body image registration using our SWMI with Gaussian-shaped weight (SWMI-GW) or SOI-based weights (SWMI-SOI) as a cost function can achieve better registration results in (a) designated image region(s) as well as faster convergence. With the theoretical foundation established, we believe SWMI could be extended to larger clinical testing.

ACKNOWLEDGMENTS

APPENDIX: DERIVATION OF SPATIALLY WEIGHTED JOINT PROBABILITY

We present the derivation of the derivative of spatially weighted joint probability. The step for derivation is the same as for the derivative of joint probability since the weights are independent of the transform parameter. This is shown as follows. First, let u be $l - f_T(g(\mathrm{x}|\mu)) - f_T^0 / \Delta b_T$ and t be $g(\mathrm{x}|\mu)$. Then, by applying the chain rule for the Eq. (12),

$$\frac{\partial p_w(l,k|\mu)}{\partial \mu} = \alpha \sum_{\mathrm{x} \in \mathbf{V}} \frac{\partial w(\mathrm{x}) \beta^{(0)} \big(k - (f_R(\mathrm{x}) - f_R^0 / \Delta b_R) \big) \beta^{(3)}(u)}{\partial \beta^3(u)}$$

$$\times \frac{\partial \beta^3(u)}{\partial u} \frac{\partial u}{\partial t} \frac{\partial t}{\partial \mu}. \tag{A1}$$

As mention above, μ is the parameter of test image. However, $w(\mathrm{x})$ and $\beta^{(0)}$ are defined on reference image domain V_R. Therefore, Eq. (A1) can be solved as

$$\frac{\partial p_w(l,k|\mu)}{\partial \mu} = \alpha \sum_{\mathrm{x} \in \mathbf{V}} \left[w(\mathrm{x}) \cdot \beta^{(0)} \left(k - \frac{f_R(\mathrm{x}) - f_R^0}{\Delta b_R} \right) \cdot \left. \frac{\partial \beta^3(u)}{\partial u} \right|_{u = l - \frac{f_T(g(\mathrm{x}|\mu)) - f_T^0}{\Delta b_T}} \cdot \frac{1}{\Delta b_T} \left(\left. \frac{-\partial f_T(t)}{\partial t} \right|_{t = g(\mathrm{x}|\mu)} \right)^T \frac{\partial g(\mathrm{x}|\mu)}{\partial \mu} \right]$$

$$= \frac{\alpha}{\Delta b_T} \sum_{\mathrm{x} \in \mathbf{V}} \left[w(\mathrm{x}) \cdot \beta^{(0)} \left(k - \frac{f_R(\mathrm{x}) - f_R^0}{\Delta b_R} \right) \cdot \left. \frac{\partial \beta^3(u)}{\partial u} \right|_{u = l - \frac{f_T(g(\mathrm{x}|\mu)) - f_T^0}{\Delta b_T}} \cdot \left(\left. \frac{-\partial f_T(t)}{\partial t} \right|_{t = g(\mathrm{x}|\mu)} \right)^T \frac{\partial g(\mathrm{x}|\mu)}{\partial \mu} \right] \tag{A2}$$

Now we can compute the derivative from the gradient of the test image, the derivative of the cubic B-spline, and the derivatives of the transform parameters.

a)Author to whom correspondence should be addressed. Electronic mail: jason.sohn@case.edu

[1]L. Xing, B. Thorndyke, E. Schreibmann, Y. Yang, T. F. Li, G. Y. Kim, G. Luxton, and A. Koong, "Overview of image-guided radiation therapy," Med. Dosim. **31**, 91–112 (2006).

[2]D. L. Hill, P. G. Batchelor, M. Holden, and D. J. Hawkes, "Medical image registration," Phys. Med. Biol. **46**, R1–R45 (2001).

[3]S. Klein, M. Staring, and J. P. Pluim, "Evaluation of optimization methods for nonrigid medical image registration using mutual information and B-splines," IEEE Trans. Image Process. **16**, 2879–2890 (2007).

[4]M. Holden, "A review of geometric transformations for nonrigid body registration," IEEE Trans. Med. Imaging **27**, 111–128 (2008).

[5]W. R. Crum, L. D. Griffin, D. L. Hill, and D. J. Hawkes, "Zen and the art of medical image registration: Correspondence, homology, and quality," Neuroimage **20**, 1425–1437 (2003).

[6]E. Schreibmann and L. Xing, "Image registration with auto-mapped control volumes," Med. Phys. **33**, 1165–1179 (2006).

[7]S. Boswell, W. Tome, R. Jeraj, H. Jaradat, and T. R. Mackie, "Automatic registration of megavoltage to kilovoltage CT images in helical tomotherapy: An evaluation of the setup verification process for the special case of a rigid head phantom," Med. Phys. **33**, 4395–4404 (2006).

[8]P. Viola and W. M. Wells III, "Alignment by maximization of mutual information," in Proceedings of the 5th International Conference Computer Vision, IEEE, (1995), pp. 16–23.

[9]A. Collignon, F. Maes, D. Delaere, D. Vandermeulen, P. Suetens, and G. Marchal, "Automatic multi-modality image registration based on information theory," in Proceedings of XIVth International Conference Information Processing in Medical Imaging — IPMI'95, 1995, Vol. **3**, 263–274.

[10]J. P. Pluim, J. B. Maintz, and M. A. Viergever, "Mutual-information-based registration of medical images: A survey," IEEE Trans. Med. Imaging **22**, 986–1004 (2003).

[11]K. J. Ruchala, G. H. Olivera, and J. M. Kapatoes, "Limited-data image registration for radiotherapy positioning and verification," Int. J. Radiat. Oncol., Biol., Phys. **54**, 592–605 (2002).

[12]F. Maes, A. Collignon, D. Vandermeulen, G. Marchal, and P. Suetens, "Multimodality image registration by maximization of mutual information," IEEE Trans. Med. Imaging **16**, 187–198 (1997).

[13]C. E. Rodríguez and M. H. Loew, "Global optimization of weighted mutual information for multi-modality image registration," in Proceedings of SPIE Medical Imaging: Image Processing, 1999, Vol. 3338, pp. 89–96.

[14]X. Liu and W. Chen, "Elastic registration algorithm of medical images based on fuzzy set," in Proceedings of the Workshop of Biomedical Image Registration, 2006 [Lect. Notes Comput. Sci. **4057**, 214–221 (2006)].

[15]D. Rueckert, M. J. Clarkson, D. L. G. Hill, and D. J. Hawkes, "Non-rigid registration using higher-order mutual information," in Proceedings of SPIE Medical Imaging: Image Processing, 2000, pp. 438–447.

[16]C. E. Rodriguez-Carranza and M. H. Loew, "Weighted and deterministic entropy measure for image registration using mutual information," in Proceedings of SPIE Medical Imaging: Image Processing, 1998, pp. 155–166.

[17]J. P. Pluim, J. B. Maintz, and M. A. Viergever, "Image registration by maximization of combined mutual information and gradient information," IEEE Trans. Med. Imaging **19**, 809–814 (2000).

[18]W. Cho, S. Kim, M. Lee, S. Kim, S. Park, and C. Jeong, "Multimodality image registration using spatial procrustes analysis and modified conditional entropy," J. Signal Process. Syst. **54**, 101–114 (2009).

[19]Z. Hou, "A review on MR image intensity inhomogeneity correction," Int. J. Biomed. Imaging **2006** (2006).

[20]K. Wilkie and E. Vrscay, in *ICIAR 2005*, Lecture Notes in Computer Science Vol. 3656, edited by M. Kamel and A. Campilho (Springer-Verlag, Berlin/Heidelberg, 2005), pp. 63–72.

[21]M. Staring, S. Klein, and J. P. Pluim, "A rigidity penalty term for nonrigid registration," Med. Phys. **34**, 4098–4108 (2007).

[22]P. Thévenaz and M. Unser, "Optimization of mutual information for multiresolution image registration," IEEE Trans. Image Process. **9**, 2083–2099 (2000).

[23]S. Guiasu, *Information Theory with Applications* (McGraw-Hill, New York, 1977).

[24]D. Mattes, D. R. Haynor, H. Vesselle, T. K. Lewellen, and W. Eubank, "PET-CT image registration in the chest using free-form deformations," IEEE Trans. Med. Imaging **22**, 120–128 (2003).

[25]J. Poletti and D. McLean, "The effect of source to image distance on scattered radiation to the image receptor," Australas. Phys. Eng. Sci. Med. **27**, 180–188 (2004).

[26]S. A. Graham, D. J. Moseley, J. H. Siewerdsen, and D. A. Jaffray, "Compensators for dose and scatter management in cone-beam computed tomography," Med. Phys. **34**, 2691–2703 (2007).

[27]L. Ibáñez, W. Schroeder, L. Ng, and J. Cates, *The ITK Software Guide* (Kitware Inc., Clifton Park, New York, 2003).

[28]E. K. Chong and S. H. Żak, *An Introduction To Optimization* (Wiley, New York, 2001).

[29]J. P. Pluim, J. B. Maintz, and M. A. Viergever, "Mutual information matching in multiresolution contexts," Image Vis. Comput. **19**, 45–52 (2001).

[30]D. C. Liu and J. Nocedal, "On the limited memory BFGS method for large scale optimization," Math. Program. **45**, 503–528 (1989).

[31]S. B. Park, M. Yao, and J. W. Sohn, "Comparison of manual plus MI registration to SWMI registration using MVCT for head-and-neck cancer patients," Med. Phys. **36**, 2482 (2009).

[32]S. B. Park, F. C. Rhee, J. I. Monroe, and J. W. Sohn, "Spatial weighted mutual information for image registration in image guided radiation therapy," Med. Phys. **35**, 2855 (2008).